Journal of Molecular Structure 1349 (2026) 143838

Contents lists available at ScienceDirect

Journal of Molecular Structure

journal homepage: www.elsevier.com/locate/molstr

Characterization of mucins, glycosaminoglycans, and bioactive compounds in *Helix aspersa's* slime by spectroscopic and biochemical analysis

Michele Ciulla [a,b], Muhammad Rashad [a,*], Mattia Spano [c], Luisa Mannina [c], Stefania Garzoli [c], Gokhan Zengin [d], Stefano Di Giacomo [a], Pantaleone Bruni [a,b], Pietro Di Profio [a], Antonella Fontana [a,b], Stefania Ferrari [a,b], Amelia Cataldi [a,b], Simone Carradori [a,b,1], Susi Zara [a,1]

[a] *Department of Pharmacy, "G. d'Annunzio" University of Chieti-Pescara, via dei Vestini 31, 66100 Chieti, Italy*
[b] *UdA-Tech Lab research center, G. d'Annunzio" University of Chieti-Pescara, 66100 Chieti, Italy*
[c] *Department of Chemistry and Technology of Drugs, Sapienza University of Rome, P.le Aldo Moro 5, 00185 Rome, Italy*
[d] *Department of Biology, Science Faculty, Selcuk University, 42130 Konya, Turkey*

ARTICLE INFO

Keywords:
Snail slime
Mucins
Glycosaminoglycans
Raman and NMR spectroscopy
FTIR-ATR
Thermal analysis

ABSTRACT

Snail slime (SS), a secretion produced by *Helix aspersa*, is a complex biological matrix rich in macromolecules has gained considerable interest due to its biologically relevant components and potential applications in medicine, cosmetics, and biotechnology. This study focuses on the chemical characterization of SS, comparing stabilized commercial slime with preservatives to a non-stabilized natural, preservative-free variant. Advanced analytical techniques, such as Attenuated Total Reflection Fourier Transform Infrared Spectroscopy, Nuclear Magnetic Resonance, Solid-Phase Microextraction Gas Chromatography-Mass Spectrometry, Raman spectroscopy, and Thermal analysis were employed to identify key metabolites and bioactive compounds. Moreover, quantitative assays were performed to evaluate the antioxidant, metal chelation and enzyme inhibition activities. Analytical techniques identified mucins, glycosaminoglycans, antimicrobial peptides, and antioxidants, with variations in composition influenced by processing methods. Quantitative assays revealed that SS possesses strong antioxidant properties, significant metal chelation capacity, and inhibitory activity against cholinesterases, tyrosinase, amylase, and glucosidase. Cellular assays further demonstrated its non-toxic nature and capacity to enhance dermal fibroblast viability. Furthermore, the stabilized commercially used SS has better composition, stability and activities compared to non-stabilized SS. Additionally, this is the first direct comparison of stabilized and non-stabilized SS, using multimethod analytical approach, and correlation of chemical composition with bioactivity. These findings underscore SS's complex composition and potential in biomedical and cosmetic applications, particularly in wound healing, antimicrobial, antioxidants, anti-aging formulations, and enzyme inhibitory therapies.

Abbreviations: SS, snail slime; GC, gas chromatography; MS, mass spectrometry; ICP-AES, inductively coupled plasma-atomic emission spectrometry; FAAS, flame atomic absorption; ATR, attenuated total reflection; FTIR, fourier transform infrared spectroscopy; NMR, nuclear magnetic resonance spectroscopy; HS-SPME/GC-MS, headspace solid phase microextraction gas chromatography-mass spectrometry; GMP, good manufacturing practices; TSP, 3-(trimethylsilyl)propionic acid sodium salt; LRIs, linear retention indices; DVB/CAR/PDMS, divinylbenzene/carboxen/polydimethylsiloxane; BSTFA, bis(trimethylsilyl)trifluoroacetamide; TIC, total ion chromatogram; DLATGS, deuterated triglycine sulphate doped with l-alanine; TGA, thermogravimetric analysis; DSC, differential scanning calorimetry; TPC, total phenolic content; GAE, gallic acid equivalents; TE, trolox equivalents; GALAE, galantamine equivalents; KAE, kojic acid equivalents; ACE, acarbose equivalents; Na_2CO_3, sodium bicarbonate; DPPH, 1, 1 diphenyl 2 picrylhydrazyl; ABTS, 2,2′-azino-bis(3-ethylbenzothiazoline)-6-sulfonic acid; $CuCl_2$, copper chloride; NH_4Ac, ammonium acetate; TPTZ, 2,4,6-tris(2-pyridyl)-*s*-triazine (TPTZ); $FeCl_3$, ferric chloride; H_2SO_4, sulfuric acid; $FeCl_2$, iron chloride; EDTA, ethylenediaminetetraacetic acid; DTNB, 5,5-dithio-bis(2-nitrobenzoic) acid; ATCI, acetylthiocholine iodide; BTCI, butyrylthiocholine iodide; KI, potassium iodide; PNPG, 4-nitrophenyl-α-D-glucopyranoside; DMEM, dulbecco's modified Eagle Medium; FBS, Fetal Bovine Serum; MTT, (3-(4,5-dimethylthiazol-2-yl)-2,5-diphenyltetrazolium bromide); DMSO, dimethyl sulfoxide.

* Corresponding author.
E-mail address: muhammad.rashad@unich.it (M. Rashad).
[1] These authors equally contributed to the paper.

https://doi.org/10.1016/j.molstruc.2025.143838
Received 18 March 2025; Received in revised form 20 August 2025; Accepted 30 August 2025
Available online 1 September 2025

1. Introduction

For the last two decades, researchers have been working on the beneficial effects of snail slime (SS) (sometimes referred as snail mucus), obtained from different species of terrestrial and marine gastropods. In the past, SS extraction was not an easy task, most of the time compromising the animal's life. Thanks to recent advanced procedures, such as cruelty-free Muller method explained by Ricci et al. [1], SS extraction is currently improved while preserving the animal's health and, at the same time, guaranteeing a richer final product.

The slime or mucus produced by the snails during their movement or from the epithelium of the dorsal and lateral foot has garnered significant attention thanks to its appreciable properties and potential applications in several fields, such as medicine, cosmetics, and biotechnology [2,3]. This viscous secretion, composed of a complex mixture of compounds, plays a crucial role in the snail's survival and has been the subject of extensive chemical characterization studies. One of the primary components of slime is mucin, a high molecular weight glycoprotein responsible for its viscous and adhesive nature [1]. Mucins are known to exhibit a diverse range of biological activities, including adhesion, lubrication, and protection against pathogens and dehydration [2,4]. Moreover, slime contains various proteins, enzymes, allantoin, glycolic acid and bioactive molecules that contribute to its unique properties [5]. In particular, it has been revealed that mucus is primarily composed of glycoproteins [6]: galactose, N-acetyl galactosamine, and N-acetylglucosamine have been identified as the major monosaccharide components [7]. Various glycosaminoglycans (GAGs), including hyaluronic acid, have been identified contributing to the mucus's rheological properties [8]. It also contains proline-rich peptides with potential antimicrobial properties, contributing to the snail's innate immune defense mechanisms [9].

Mucus obtained from *Helix aspersa* and *Eremina desertorum* showed significant antioxidants, antityrosinase, and anticancer activities against epithelioid carcinoma (HeLa) [10]. The lipid fraction has been found to exhibit antimicrobial and antioxidant activities, making it an attractive candidate for biomedical applications [11]. Lastly, the inorganic components, particularly calcium and iron, have been implicated in its self-healing and adhesive properties leading to the development of adhesives and self-healing materials inspired by the unique composition of *Helix aspersa* slime [12].

Chemical analysis of SS has attracted great interest in recent years due to its potential uses in several sectors. Through various analytical techniques, several bioactive compounds present in *Helix aspersa* slime have been identified. Antimicrobial and antifungal peptides, such as achasin and helix amides mytimacin-AF, have been isolated and characterized from *A. fulica* [13,14]. Additionally, chemical analysis let to identify the presence of antioxidants, including polyphenols and flavonoids [15].

Advancements in analytical techniques have facilitated more comprehensive investigations into the SS chemical composition. Vassilev et al. [16] used MS and NMR to identify over 20 metabolites in the slime of *Helix aspersa*, providing insights into its potential biological functions [16]. Additionally, GC–MS was employed to determine the nine most abundant chemicals from mucus of *Monacha obstructa, Theba pisana* and *Eobania vermiculata*. Results revealed that hexamethylcyclotrisiloxane and methoxy phenyl oxime having molecular weight 222.06 and 151.06, respectively, were the major components found in mucus of all snail species [17]. In addition, the content of trace elements in *A. fulica* slime was determined by ICP-AES and FAAS revealing the abundance of Ca, Mg, Fe, Zn, Cu, and Co [6,18].

In our previous study we focused on the biological effect of SS on human gingival fibroblasts finding its capability, on one hand to promote cell survival and angiogenesis and, on the other hand, to counteract inflammation [1].

Building on our previous findings, the present study aims to further deepen the chemical and biological characterization of *Helix aspersa* mucus. The main objective is the qualitative and quantitative identification of its main bioactive components using cutting-edge techniques, from FTIR, NMR, HS-SPME/GC-MS, thermal analysis and GC-MS to the most advanced Raman spectroscopy analysis, able to get data from both unprocessed and therefore non-destructive and processed samples.

Notably, some of the employed methodologies, such as Raman spectroscopy and thermal analisys are applied here for the first time to SS analysis, while others like FTIR-ATR and headspace-SPME/GC-MS are used in a more detailed and integrated way than in previous literature. These innovative approaches allow for a high-resolution characterization of mucins, glycosaminoglycans, organic acids, peptides, and volatile compounds.

In parallel, we performed a comparative analysis between two SS formulations: natural sample and a stabilized sample. Through a series of biochemical and biological assays, including antioxidant activity, radical scavenging, enzyme inhibition, and dermal fibroblast viability, we assessed how the stabilization process affects slime composition and functionality. These evaluations are highly relevant in light of the requirements for cosmetic GMP and product shelf-life. Understanding the effect of preservatives on SS bioactivity is essential to its use as a cruelty-free, stable, and functional raw material for formulations in cosmetics, dermatology, wound healing, and tissue regeneration. A schematic overview of the experimental workflow is presented in Figure 1.

2. Materials and methods

2.1. SS extraction and processing

Live healthy snails *H. aspersa,* aged 12–15 months, were pre-washed in running water at room temperature in order to remove the dust and debris as well as awaken the animal. Washed snails were then transferred to Muller extractor where they first received an antimicrobial treatment with ozonated water shower followed by 10 % citric-acid stimulated slime extraction for 30 minutes each. The extracted slime (natural and non-stabilized SS) was collected and filtered through 0.2 μm filter and mixed with sodium benzoate (0.1 %) and potassium sorbate (0.1 %) preservatives to be suitable for the market and other industrial processing (commercial and stabilized SS). The final products were stored in the dark at +4 °C to be used within six months.

2.2. Sampling

Samples of SS (with or without the addition of two preservatives) were kindly provided by Lumacheria Italiana srl. Cherasco, Italy. Samples were freeze-dried with a Buchi Lyovapor L-200 at -55°C and 0.200 mbar conditions obtaining a solid residue weight of 21.5 mg and 24.8 mg from 1 mL of slime without (non-stabilized) and with preservatives (stabilized), respectively.

2.3. NMR analysis

After drying 2 mL of SS, the solid residue was solubilized in 700 μL phosphate buffer/D_2O (200 mM) with 0.3 mM TSP as an internal standard for metabolite measurement. The resulting solution was placed into a 5 mm NMR tube and analyzed using a Jeol JNM-ECZ 600R (JEOL Ltd., Tokyo-Japan) with a JEOL 5 mm FG/RO DIGITAL AUTOTUNE probe and at 600.17 MHz proton frequency. To identify metabolites, one-dimensional ^{1}H and two-dimensional ^{1}H-^{1}H TOCSY, ^{1}H-^{13}C HSQC, and ^{1}H-^{13}C HMBC experiments were performed under the identical circumstances as previously described [19]. JEOL Delta software (version 5.3.1) was used to analyze spectra and integrate metabolite signals. Each sample included five replicates, and quantitative data were presented as mean value ± SD μg/mL of SS.

2.4. GC-MS analysis

Volatile metabolites were analyzed using a Perkin Elmer Clarus 500 GC system (Waltham, MA-USA) interfaced with an MS and fitted with FID detector. Separation was achieved on an Agilent VF-1ms capillary column (60 m × 0.32 mm ID, 1.0 µm DF; nonpolar 100 % dimethylpolysiloxane stationary phase). The oven program was set from 40 to 220°C at a ramp of 6°C/min, with a final hold of 15 min. Helium was used as carrier gas (1 mL/min, constant flow). Electron ionization was performed at 70 eV, and spectra were recorded in the 40–500 m/z range. Compounds were identified by matching mass spectra against the Nist 11 library and by comparing calculated LRIs, obtained using n-alkanes (C_8–C_{25}), with reference values reported in the Nist Chemistry WebBook. Relative abundances of constituents were determined from FID peak areas (mean of triplicate analyses), without applying correction factors or internal standards.

2.5. SPME sampling

To determine the volatile content of all slime samples, solid-phase microextraction (SPME) was performed. The extraction process of volatiles was carried out on a SPME device from Supelco (Bellefonte, PA) with 1 cm fiber coated with 50/30 µm DVB/CAR/PDMS. After reaching the equilibrium phase, the fiber was exposed to the headspace of the

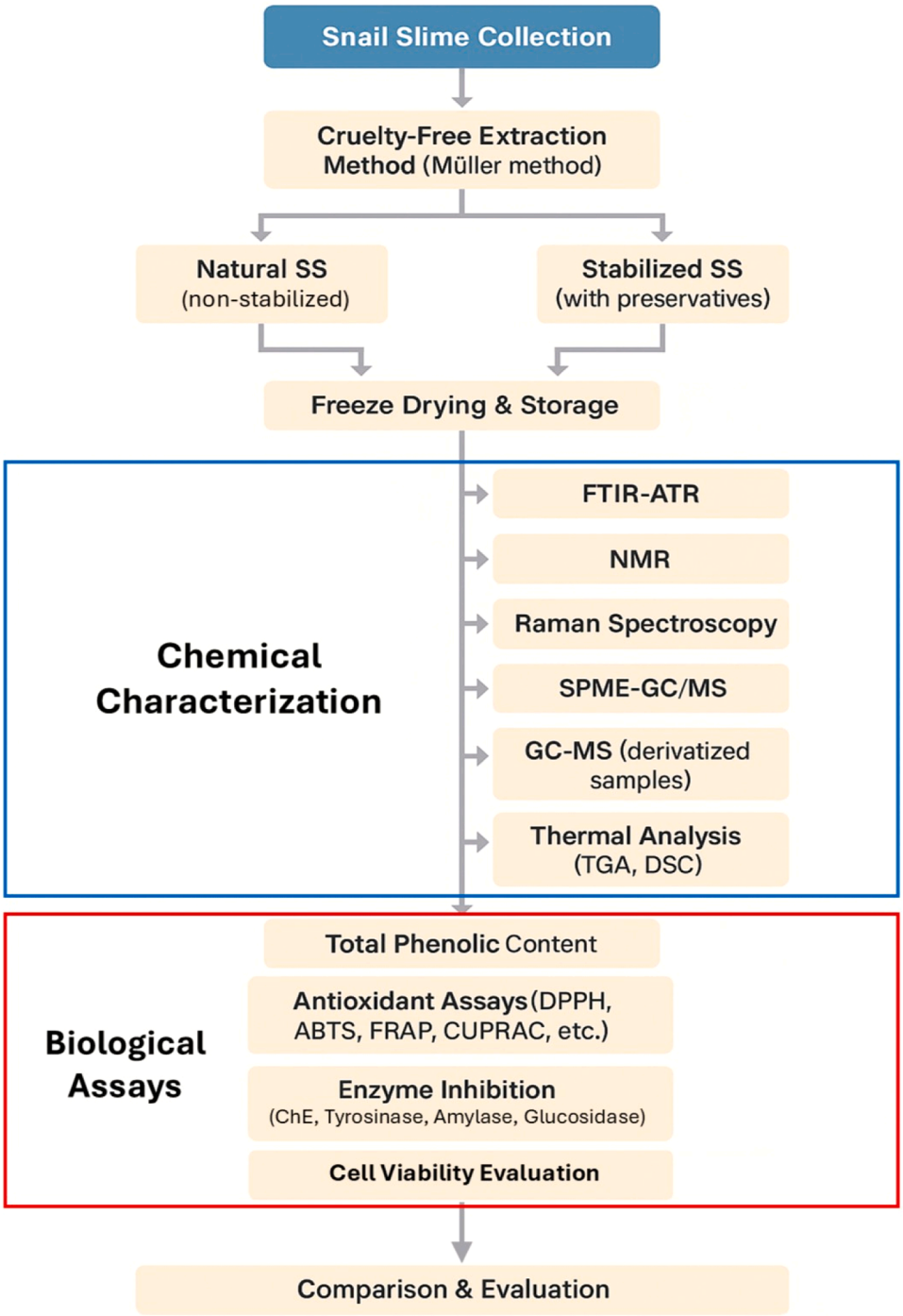

Fig. 1. Schematic representation of the experimental workflow.

samples maintained at 40°C for 25 min. Finally, the analytes were thermally desorbed in a splitless GC injector set to 250°C. The applied operative conditions of gas chromatographic and mass spectrometer were as reported in the previous section. The analyses were carried out in duplicate.

2.6. GC-MS Analysis of derivatized samples

For compositional profiling of stabilized and non-stabilized freeze-dried SS, nearly 0.5 mg of each sample were mixed with 50 μL BSTFA and 150 μL pyridine. For 30 min, the mixture was heated at 70°C, and 1 μL of the silylated sample was manually injected into the GC (injector temperature 270°C, splitless mode). Oven was programmed as follows: initial 70°C, ramped at 6°C/min to 170°C (hold 1 min), then 8°C/min to 250°C (hold 30 min). Mass spectra were acquired under electron ionization. Compound identification was performed using the Nist library, considering both similarity scores and relative contribution to the TIC. Quantification was based on electronic integration of GC-FID peak areas, without internal standards or response factor adjustments. All analyses were performed in duplicate.

2.7. FTIR-ATR analysis

Infrared spectra were collected using a Shimadzu IRAffinity-1S FTIR spectrophotometer (Shimadzu Italia S.r.l., Milan, Italy) with a sealed, desiccated interferometer, a DLATGS detector, and a single-reflection diamond ATR crystal (QATR 10, Shimadzu Italia S.r.l., Milan-Italy). Measurements were taken within the spectral range of 4000–400 cm^{-1} by averaging 45 interferograms at a resolution of 4 cm^{-1}, applying Happ–Genzel apodization on lyophilized samples. Data acquisition was carried out over the spectral range of 4000–400 cm^{-1}, averaging 45 interferograms at a resolution of 4 cm^{-1}, with Happ–Genzel apodization applied to lyophilized samples. The ATR crystal was thoroughly cleaned before each measurement, and a new background spectrum was recorded for every sample. Each measurement was performed in triplicate. Spectral processing and analysis were conducted using LabSolution IR software (version 2.27, Shimadzu Italia S.r.l., Milan-Italy).

2.8. Raman measurements

Raman spectra were recorded using a high-performance confocal Raman microscope (XploRA PLUS, HORIBA, Japan) equipped with a deep-cooled CCD detector. The LabSpec software (version 6.6.1.14, HORIBA, Japan) was used for data acquisition, optimization, and initial processing, while further refinements and analyses were conducted with Origin 8.5. Due to the strong florescence of fresh samples, all the Raman spectra were recorded on lyophilized samples. The measurements covered the spectral range of 400–3400 cm^{-1}, employing an 1800-line/mm grating. A single spectrum was obtained from the lyophilized sample using a 532 nm laser, with an exposure time of 30 seconds and 5 accumulations to minimize the risk of sample overheating.

2.9. Thermal analysis

TGA were performed using the Discovery SDT 650 (TA Instruments, Waters). To achieve proper sample stabilization, an initial conditioning isotherm was applied, followed by a heating ramp at a rate of 10°C/min up to a maximum temperature of 900°C. The measurements were carried out under N_2 and air atmospheres to evaluate the thermal behavior of the materials in controlled environments. Throughout the analysis, the gas flow rate was maintained at a constant 100 mL/min to ensure reproducibility and reliability of the results. The data collected were processed using TRIOS software.

DSC analysis was conducted on the commercial stabilized SS samples by using a *Discovery DSC 25* (TA Instruments, Waters), with *TRIOS Software* employed for experimental control, data acquisition, and analysis. For the freeze-dried (lyophilized) slime samples, the procedure involved heating at a rate of 10°C/min, starting from the storage temperature of 4°C reaching setpoints of 20°C, 25°C, 30°C, 35°C, 40°C, 50°C, 70°C, 80°C, 90°C, and 100°C. An isothermal hold of 1 minute was maintained at each target temperature to ensure complete thermal equilibration of the sample. The cooling phase was conducted at 10°C/min, returning the sample to the initial temperature. This temperature sequence was applied for a single cycle, while extended stability testing involved 20 cycles up to a maximum temperature of 70°C to avoid potential degradation of the material. For the stabilized slime (liquid) samples, the protocol followed a similar heating rate of 10°C/min. The temperature setpoints were 20°C, 25°C, 30°C, and 35°C with an isothermal hold of 1 minute each. For stability testing, the cycles extended to 40°C and 50°C. All experiments were replicated thrice to ensure reliability and reproducibility of the results.

2.10. Assays for total phenolic content

Phenolic constituents were quantified using modified Folin–Ciocalteu protocol [20]. In brief, 0.25 mL of sample were mixed with 1 mL of diluted Folin–Ciocalteu reagent (1:9, v/v). After 3 min, 1 % Na_2CO_3 (0.75 mL) was introduced, and the mixture was kept for 2 h at room temperature. The absorbance was recorded at 760 nm, and the results were calculated according to Eq. 1 and reported as mg GAE/g.

$$TPC = \frac{c \times V}{m} \quad (1)$$

Where, c = gallic acid concentration (mg/mL), V = sample volume (mL), m = sample mass (g).

2.11. Determination of antioxidant effects

2.11.1. Radical scavenging abilities

2.11.1.1. DPPH radical scavenging ability. Sample solution was added to 4 mL of a 0.004 % methanol solution of DPPH. The absorbances were read at 517 nm after a 30 min incubation at room temperature in the dark. DPPH radical scavenging activity was calculated according to Eq. 2 and expressed as mg TE/g sample [21–23].

$$\text{Inhibition activity } (\%) = \frac{Ac \times As}{Ac} \times 100 \quad (2)$$

Where, Ac = absorbance of control, As = absorbance of sample.

2.11.1.2. ABTS radical scavenging ability. $ABTS^{\cdot+}$ radicals were prepared by incubating the ABTS (7 mM) with potassium persulfate (2.45 mM) for 12–16 h in the dark. The solution obtained was then diluted with methanol to get the desired absorbance (0.700 ± 0.02) at 734 nm. The sample was then mixed with 2 mL of this reagent, followed by an incubation for 30 min at 25°C. The absorbance was recorded at 734 nm and percent inhibition was reported as mg TE/g and measured by using Eq. 2 [24].

2.11.2. Reducing power assays

2.11.2.1. Cupric ion reducing activity (CUPRAC). Samples were reacted with CUPRAC reagent ($CuCl_2$ 10 mM, neocuproine 7.5 mM, and 1 M NH_4Ac buffer, pH 7.0). After 30 min incubation, absorbance was taken at 450 nm. Activities were calculated according to Eq. 2 and expressed as mg TE/g [25].

2.11.2.2. Ferric reducing antioxidant power (FRAP). The premixed FRAP reagent (10 mM TPTZ in 40 mM HCl; 20 mM $FeCl_3$, 0.3 M acetate buffer, pH 3.6 at 1:1:10 v/v/v) was reacted with the sample and allowed to incubate. After 30 min, the absorbance was determined at 593 nm. Antioxidant power was expressed as mg TE/g and calculated according

to Eq. 2 [26].

2.11.2.3. Phosphomolybdenum assay. After the addition of reagent solution (28 mM sodium phosphate, 0.6 M H_2SO_4, and 4 mM ammonium molybdate), the samples were set to incubate for 90 mins at 95°C. At 695 nm, absorbance was taken, and Eq. 2 was used to represent antioxidant activity as mmol TE/g [27].

2.11.3. Metal chelating abilitiy

Chelating ability was tested by mixing the sample with $FeCl_2$ (2 mM) and initiating the reaction with 5mM ferrozine, followed by 10 min incubation. Absorbance was recorded at 562 nm, and metal chelating ability as EDTA equivalents (mg EDTAE/g) was measured according to Eq. 2 [28].

2.12. Enzyme inhibitory assays

2.12.1. Cholinesterase (ChE) inhibitory assays

Samples were incubated with DTNB and either AChE or BChE in Tris–HCl buffer (pH 8.0) at 25°C for 15 min. Reactions were started with the addition of ATCI and BTCl, respectively. Absorbance was taken at 405 nm after 10 min, and inhibition activities were expressed as mg GALAE/g, determined by Eq. 2 [29].

2.12.2. Tyrosinase inhibitory assay

Samples were reacted with tyrosinase and phosphate buffer (pH 6.8) and allowed to incubate at 25°C for 15 min before initiating the reaction by adding L-DOPA. After 10 min, the absorbance was taken at 492 nm. Percent inhibition was measured by Eq. 2 and indicated as mg KAE/g [30].

2.12.3. α-Amylase inhibitory assay

Samples were pre-incubated for 10 min with α-amylase in phosphate buffer with 6 M NaCl (pH 6.9) at 37°C. The reaction was started by the addition of 0.05 % starch solution and allowed to incubate for 10 min at 37°C. The reaction was then stopped with the addition of 1 M-HCl followed by iodine–KI reagent. Absorbance was taken at 630 nm. Eq. 2 was used to measure the percent inhibition and indicated as mmol ACE/g [31].

2.12.4. α-Glucosidase inhibitory assay

Samples were incubated for 15 min with α-glucosidase in phosphate buffer (pH 6.8), glutathione and PNPG at 37°C. 0.2 M Na_2CO_3 was used to stop the reaction. Absorbance was taken at 405 nm, and percent inhibition was calculated according to Eq. 2, indicated as mmol ACE/g [32].

2.13. Cell culture and treatments

Normal human dermal fibroblasts (NHDFs), catalog no. c-12302, purchased from Merck Life Science, (Milan, Italy) were cultured in high-glucose DMEM, supplemented with 10 % FBS and 1 % penicillin/streptomycin at 37 °C with 5 % CO_2. NHDFs, at passages 6-8, were seeded at 8000/well/200 μL density in tissue culture treated 96 well plate for overnight. Next day, cells were treated with different dilutions of SS 1:40, 1:60, and 1:80 in DMEM, the control was established as sample receiving two preservatives (sodium benzoate and potassium sorbate) and stimulating solution (citric acid).

2.14. MTT assay

Cell metabolic activity was measured according to the protocol used by Ricci et al. [1] with mild alterations using MTT assay (Merck Life Science, Budapest, Hungary) after 24 and 48 h of NHDFs treatment in the presence of SS. At the established experimental times (24 and 48 h), culture media was removed from each well of 96-well plate and cells were refed with 100 μL of 10 % MTT reagent (0.5 mg/mL) in DMEM and incubated for 5 h in the dark at 37 °C. After the said time, MTT reagent was replaced with 100 μL DMSO and incubated again for 20 minutes at 37 °C. The absorbance was taken using a synergy HT microplate reader (BioTek, Winooski, Vermont, USA) at wavelength 540 nm and percent cell viability was measured by comparing each treatment group with the control, previously adjusted at 100 %.

2.15. Statistical evaluation

The results of repeated readings were combined and displayed as mean ± SD. The student t-test (α=0.05) was used to compare the samples. Differences at $p < 0.05$ were considered significant. The analysis was performed using the statistical software GraphPad (9.0).

3. Results and discussion

3.1. NMR analysis

NMR metabolomics offers the opportunity to have a view, with a single experiment, of several metabolites classes present in slime samples observing potential qualitative and/or quantitative differences as results of slime production and process. Seven organic acids (acetate, succinate, citrate, fumarate, formate, sorbate, benzoate), alanine, betaine, and glucose were identified and quantified in the ^{1}H NMR spectra, Fig. 2, using information obtained by ^{1}H experiments (signal chemical shifts, multiplicity, *J* coupling constants), two-dimensional experiments (spin correlations), and literature data regarding a previous NMR-based analysis of *Helix aspersa* mucus [16]. The list of identified metabolites is reported in Table 1, together with ^{1}H NMR signals used for quantification and corresponding quantitative results.

Stabilized and non-stabilized samples were characterized by the same qualitative metabolite profile, showing differences from a quantitative point of view. In particular, citrate was measured as the most abundant metabolite in both samples, with the highest amount measured in non-stabilized slime. This metabolite is routinely added during industrial production to chemically stimulate slime secretion. Sorbate and benzoate were also measured in high concentrations, with stabilized slime being characterized by a two-time higher amount of these metabolites as expected, since these two molecules are used for their stabilizing properties. Regarding the other detected metabolites, stabilized slime showed higher concentrations respect with non-stabilized one, with the only exception of fumarate and alanine, although with no significative variability.

The obtained results underlined that the processing approach can

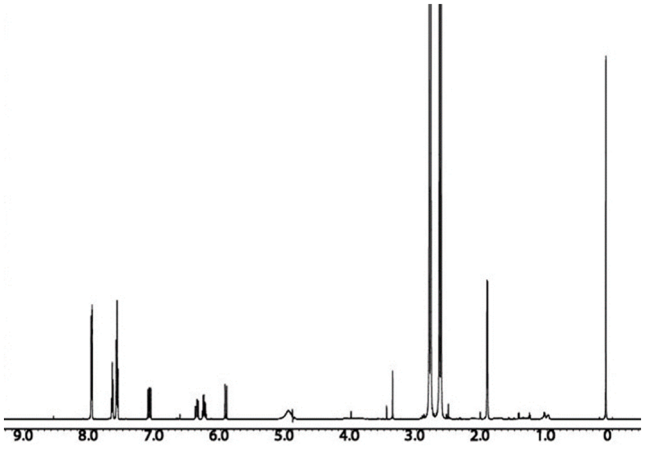

Fig. 2. 600.17 MHz ^{1}H NMR spectrum of stabilized SS in 200 mM phosphate buffer/D_2O containing 0.3 mM TSP.

Table 1
Metabolites identified in the ^{1}H spectra of SS, together with signal used for quantification (chemical shift, multiplicity, *J* coupling constant) and quantitative results expressed as μg/mL of slime (mean value ± SD).

Metabolite	^{1}H ppm, multiplicity *J* [Chen, #42]	Stabilized slime	Non-stabilized slime
Acetate	1.92, s	18.00 ± 1.38	16.63 ± 1.59
Succinate	2.41, s	44.46 ± 1.07*	14.85 ± 0.43
Citrate	2.55, d [15.3]	51893.59 ± 4515.05*	64198.46 ± 2212.68
Fumarate	6.53, s	28.50 ± 1.89	51.72 ± 1.22
Formate	8.46, s	11.84 ± 1.26	5.41 ± 0.56
Sorbate	5.83, d [15.3]	547.76 ± 8.80*	282.44 ± 18.24
Benzoate	7.88, d [7.1]	1052.05 ± 15.38*	478.79 ± 16.98
Alanine	1.48, d [7.2]	7.09 ± 0.27	9.25 ± 0.40
Betaine	3.27, s	68.07 ± 5.67*	25.95 ± 0.26
Glucose	4.66, d [8.1]	16.09 ± 0.15	6.55 ± 0.35

* Significative difference respect to no stabilized slime, ($p < 0.05$).

strongly affect the chemical profile of SS, thus affecting the potential properties and application. This behavior has been previously observed in SS with different molecular weights [16] and raw slime with or without Au nanoparticles [33].

3.2. SPME-GC/MS analyses

SPME-GC/MS technique allowed the identification and semi-quantification of 13 components in total belonging to different chemical classes and listed in Table 2. Organic acids, such as sorbic acid and benzoic acid were the most abundant in the stabilized and non-stabilized freeze-dried slime samples and in the latter traces of fatty acids were also detected. In stabilized slime benzoic acid reached the highest percentage mean value (69.4 %) followed by 2,4-dimethylbenzaldheyde (17.7 %). Further, vanillin was found in stabilized (4.8 %) and non-stabilized (8.4 %) slime. On the other side, non-stabilized slime was characterized by benzene as the major component (43.8 %). Relevant amounts of 1,3-dioxolane (16.1 %) and methoxy phenyl oxime (23.2 %) were detected only in this sample. The obtained results demonstrate how the treatment of the sample can affect its final composition. Consequently, it can be asserted that the applied analytical techniques are suitable for highlighting the effects due to different processes performed on the same matrix. To the best of our knowledge, this is the first work where an investigation of the volatile profile of the SS by Headspace-SPME-GC/MS analysis was performed. The chromatograms are reported in Figures 10-13 (Supplementary data).

The analysis conducted on the derivatized samples of stabilized and non-stabilized freeze-dried slime showed the presence of furan derivative compounds such as 2,5-furandione, 3-methyl- and 2-furoic acid which were the most representative (Table 3). The chromatograms are reported in Figures 14 and 15 (Supplementary data).

Table 3
Metabolites identified (percentage mean values ± SD) in the stabilized and non-stabilized freeze-dried SS after derivatization as determined by GC-MS.

Metabolite	Stabilized slime freeze-dried	Non-stabilized slime freeze-dried
3-methyl-2,5-furandione	18.8± 0.14	67.0± 2.52
sorbic acid	12.3± 0.08	tr
2-furoic acid	27.1± 0.21	19.9± 0.32
benzoic acid	7.2	12.3
D-lyxose	0.4	0.8
methyl 3-(3,5-di-tert-butyl-4-hydroxyphenyl) propionate	34.3	-

-: not detected.

3.3. FT-IR results

IR spectroscopy enables the identification of characteristic molecular bond vibrations, providing valuable insights and confirmations regarding the presence of specific chemical structures within the SS [34] (Fig. 3 and Table 4).

In particular, the peak at 516 cm^{-1} likely corresponds to skeletal bending modes, which are typically associated with polysaccharides and other complex carbohydrates. Similarly, the peak at 594 cm^{-1} could be linked to out-of-plane bending vibrations of the C–H bonds in polysaccharides or glycosidic linkages. The 651 cm^{-1} and 682 cm^{-1} peaks may be assigned to C–S stretching modes, possibly arising from sulfur-containing compounds such as cysteine residues in proteins. The peaks around 798 cm^{-1} and 887 cm^{-1} likely indicate C–C and C–O bending in polysaccharides, suggesting an important contribution from mucopolysaccharides. The peak at 933 cm^{-1} may correspond to C–H rocking in carbohydrate backbones, while the presence of a peak at 1126 cm^{-1}, assigned to C–O stretching in glycosylated proteins, highlights the contribute of glycoproteins in the matrix of SS. At 1198 cm^{-1}, the amide III band is present, characteristic of protein content, confirming the secondary structure of proteins, predominantly α-helices. The peak at 1323 cm^{-1} can be linked to symmetric CH_2 bending and N–H deformation, typical in amino acid side chains and polysaccharides. The broad peak at 1400 cm^{-1} corresponds to vibrations of sugars and amino acid chains, while the 1581 cm^{-1} peak is assigned to amide II, which arises from N–H bending and C–N stretching vibrations in proteins. The peak at 1700 cm^{-1} is attributed to C=O stretching, likely influenced by the citric acid used in the extraction process. However, this peak may also include contributions from C=O bonds present in other molecules containing carboxyl groups, such as amino acids. The 2538 cm^{-1} peak, though uncommon, might indicate weak hydrogen-bonded SH groups or other unknown interactions. Aliphatic C-H stretching vibrations are evident at 2947 cm^{-1}, while aromatic C–H stretching at 3078 cm^{-1} is indicative of phenyl groups, confirming protein aromatic residues. Lastly, the broad peak at 3417 cm^{-1} corresponds to O–H stretching, confirming the presence of hydroxyl groups associated with water,

Table 2
Metabolites identified (percentage mean values ± SD) in all samples of SS as determined by SPME-GC/MS technique.

Metabolite	LRI^{exp}	LRI^{lit}	Stabilized freeze-dried slime	Non-stabilized freeze-dried slime	Stabilized slime	Non-stabilized slime
1,3-dioxolane	588	590	-	-	-	16.1± 1.05
2-methyl-furan	600	605	-	-	-	6.6± 0.05
Benzene	660	663	-	-	-	43.8± 2.01
N-ethylformamide	701	706	-	-	-	1.9± 0.07
sorbic acid	1050	1056	27.8± 0.12	24.7± 0.20	-	-
2,4-dimethylbenzaldheyde	1185	1181	-	-	17.7± 1.02	-
benzoic acid	1193	1191	72.2± 1.35	71.9± 1.28	69.4± 1.21	-
methoxy phenyl oxime	1305	1301	-	-	-	23.2± 1.04
Vanillin	1414	1410	-	-	4.8± 0.04	8.4± 0.08
3,5-di-*t*-butylphenol	1560	1555	-	-	8.1± 0.05	-
tridecanoic acid	1662	1658	-	0.5± 0.02	-	-
oleic acid	2148	2151	-	1.0± 0.03	-	-
stearic acid	2182	2187	-	1.8± 0.04	-	-

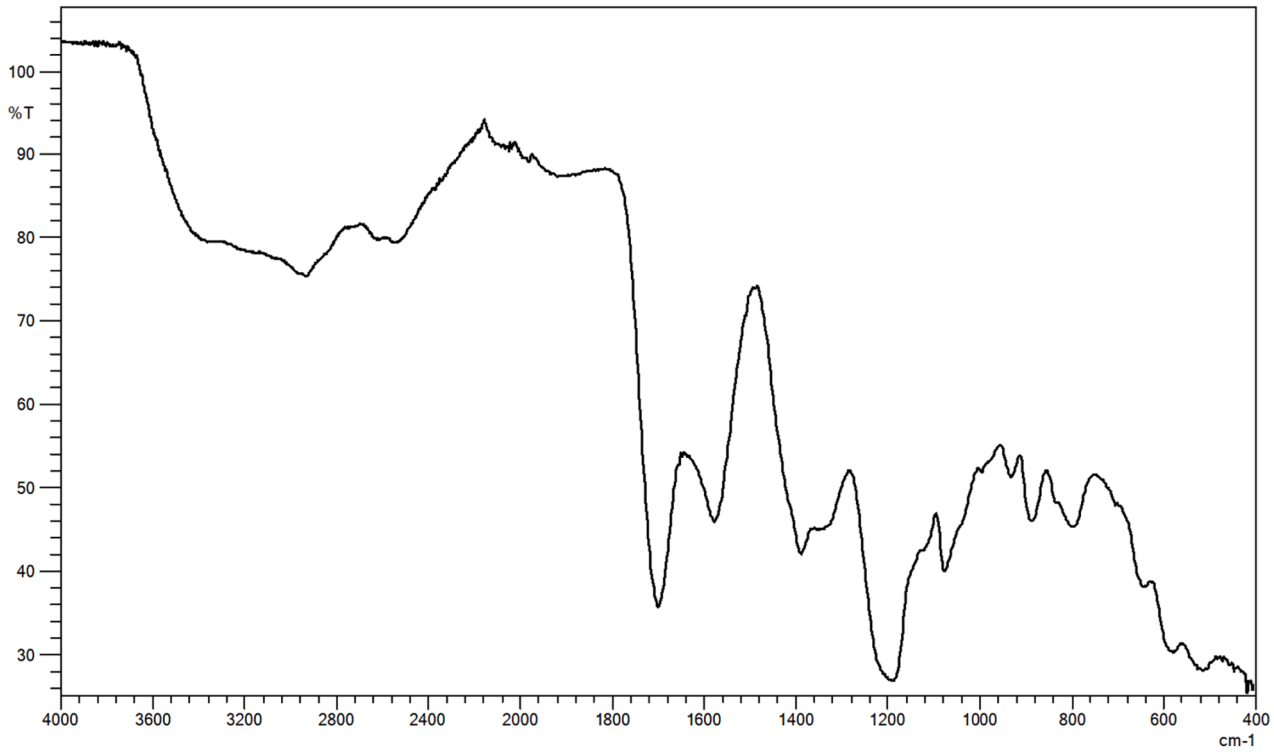

Fig. 3. FT-IR spectrum of stabilized SS in the lyophilized form.

Table 4
Infrared absorption bands and their corresponding vibrational modes identified in the sample.

Wavenumber (cm^{-1})	Vibration Type	Molecules
516	Skeletal bending	Polysaccharides, complex carbohydrates
594	Out-of-plane C–H bending	Polysaccharides, glycosidic linkages
651, 682	C–S stretching	Sulfur-containing compounds, cysteine residues (proteins)
798, 887	C–C and C–O bending	Mucopolysaccharides
933	C–H rocking	Carbohydrate backbones
1126	C–O stretching	Glycosylated proteins, glycoproteins
1198	Amide III (secondary structure)	Proteins (predominantly α-helices)
1323	Symmetric CH_2 bending, N–H deformation	Amino acids, polysaccharides
1400	Vibrations of sugars and amino acid chains	Sugars, amino acids
1581	Amide II (N–H bending, C–N stretching)	Proteins
1700	C=O stretching	Citric acid (from the industrial process)
2538	Weak hydrogen-bonded SH groups or unknown interactions	Possible thiol-containing compounds
2947	Aliphatic C–H stretching	Lipids, proteins
3078	Aromatic C–H stretching	Phenyl groups (protein aromatic residues)
3417	O–H stretching	Hydroxyl groups (water, polysaccharides, glycoproteins)

tr: percent mean value <0.1 %.

polysaccharides, and glycoproteins.

3.4. Raman results

The Raman spectrum analysis of SS revealed distinct peaks that provide valuable insights into its biochemical composition (Fig. 4 and Table 5).

The characteristic peak at 369 cm^{-1} could correspond to skeletal modes or lattice vibrations, often seen in polysaccharides or other complex carbohydrates. The peak at 684 cm^{-1}, attributed to OCN bending (Amide IV-VII), indicates the presence of protein backbones, a key structural component of mucin glycoproteins. Notable peaks at 795 cm^{-1} and 877 cm^{-1} correspond to C–C or C–O stretching vibrations and indole ring vibrations, respectively. The former is characteristic of

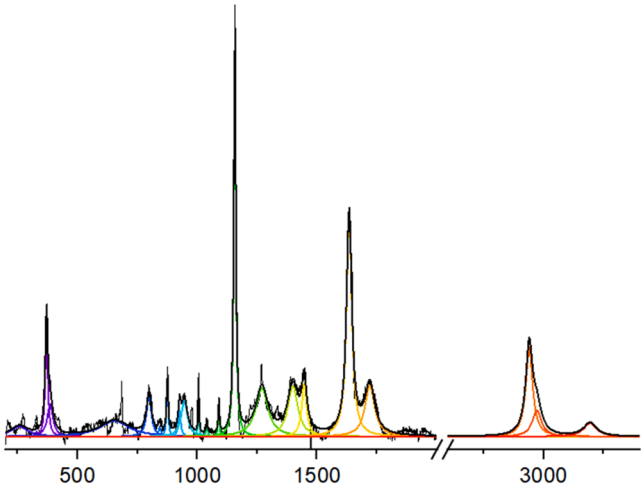

Fig. 4. Raman spectrum of stabilized and lyophilized SS. The black line represents the raw spectrum, the colored lines correspond to the individual deconvoluted components.

Table 5
Raman peak assignments for stabilized and lyophilized SS. The table reports the Raman shift (cm^{-1}), the relative assignment and the corresponding species.

Raman Shift	Assignment	Species
369 cm^{-1}	lattice vibrations	Polysaccharides
684 cm^{-1}	OCN bending	Amide IV-VII
795 cm^{-1}	Indole ring vibration	Tryptophan
877 cm^{-1}	Indole ring vibration	Tryptophan
1005 cm^{-1}	Benzene ring breathing	Phenylalanine
1092 cm^{-1}	C–O stretching	Carbohydrates
1157 cm^{-1}	Indole ring	Tryptophan
1268 cm^{-1}	Amide III	Proteins
1390 cm^{-1}	N-C-N Imidazole	Histidine
1449 cm^{-1}	C-H deformation	Alkyl chains
1630 cm^{-1}	Amide I	Random coil (Hexamer in crystalline phase)
1717 cm^{-1}	C=O Stretch.	Citric acid and other carboxylic groups
2943 cm^{-1}	C-H_{sym} aliphatic stretching	Fatty acid chains
2990 cm^{-1}	C-H_{asym} aliphatic stretching	Fatty acid chains
3078 cm^{-1}	C-H aromatic stretching	Aromatic amino acids
3195 cm^{-1}	N-H stretching	Amides (proteins)

β-glycosidic linkages in mucopolysaccharides, while the latter indicates the presence of tryptophan residues, often involved in protein stability and interactions. The peak at 1005 cm^{-1}, linked to benzene ring breathing, confirms the presence of phenylalanine, another aromatic amino acid contributing to protein folding and function. Additionally, the peak at 1092 cm^{-1} likely represents C–O stretching, a characteristic vibration of carbohydrates, further confirming the presence of sugar moieties in mucins or glycosaminoglycans. The peak at 1157 cm^{-1} is attributed to indole ring vibrations from tryptophan. The amide III band at 1268 cm^{-1} and the amide I band at 1630 cm^{-1}, the latter typically associated with α-helices and random coil structures, further highlight the dominance of proteinaceous components in the slime. The peak at 1390 cm^{-1}, corresponding to N-C-N vibrations, while the peak at 1449 cm^{-1} could correspond to CH_2/CH_3 deformation, commonly associated with lipids or fatty acid chains, which may be present in small amounts, contributing to the slime's hydrophobic properties. As confirmed by the FTIR spectra, the peak at 1717 cm^{-1}, assigned to C=O stretching, is related to the presence of the citric acid used during the extraction process. The aliphatic symmetric and asymmetric C-H stretching modes (2943 cm^{-1}, 2990 cm^{-1}, respectively) confirm the presence of hydrocarbon chains, indicative of lipid components or carbohydrate moieties within mucopolysaccharides. The aromatic C-H stretching at 3078 cm^{-1} might indicate the existence of aromatic amino acid residues like tryptophan, phenylalanine, and tyrosine. Lastly, the broad N-H stretching peak at 3195 cm^{-1} highlights the contribution of amides, further supporting the significant role of proteins. Since the samples analyzed were dried (lyophilized), we did not observe the classical signal of water at 3100-3400 cm^{-1}.

3.5. Thermal analysis

The thermogravimetric analysis of freeze-dried SS gives some insight into the thermal decomposition behavior of the sample under different atmospheres (air and nitrogen). The data show distinct differences in mass loss profiles between the two environments, reflecting the effects of oxidation in air and pyrolysis in nitrogen [35] (see Fig. 5).

At low temperatures (35-175°C), significant mass losses are observed in both atmospheres. These initial losses are consistent with the behavior of volatile and hygroscopic compounds present in the sample such as cyclic ethers and furans, along with the removal of residual water. As the temperature increases (300-550°C), the decomposition of organic acids and aromatic compounds becomes evident. In air, the oxidation process accelerates the breakdown of compounds such as benzoic acid and other aromatic derivatives, leading to a significant mass loss in this range. In nitrogen, the pyrolysis of organic acids and simpler aromatic compounds occurs, resulting in similar mass losses, although the decomposition may be less complete compared to air. In the temperature range of 550-600°C, the decomposition of more stable compounds such as long-chain carboxylic acids and phenolic derivatives is observed in both atmospheres. In air, this process is facilitated by oxidation, while in nitrogen, the decomposition proceeds via pyrolysis. At higher temperatures (600-800°C), the degradation of lipids and other complex aromatic compounds is evident. In air, oxidation leads to the combustion of these compounds, while in nitrogen, the process is slower and results in the formation of carbonaceous residues. At temperatures above 800°C, the decomposition continues with the release of more stable components, including inorganic salts. In air, this is likely related

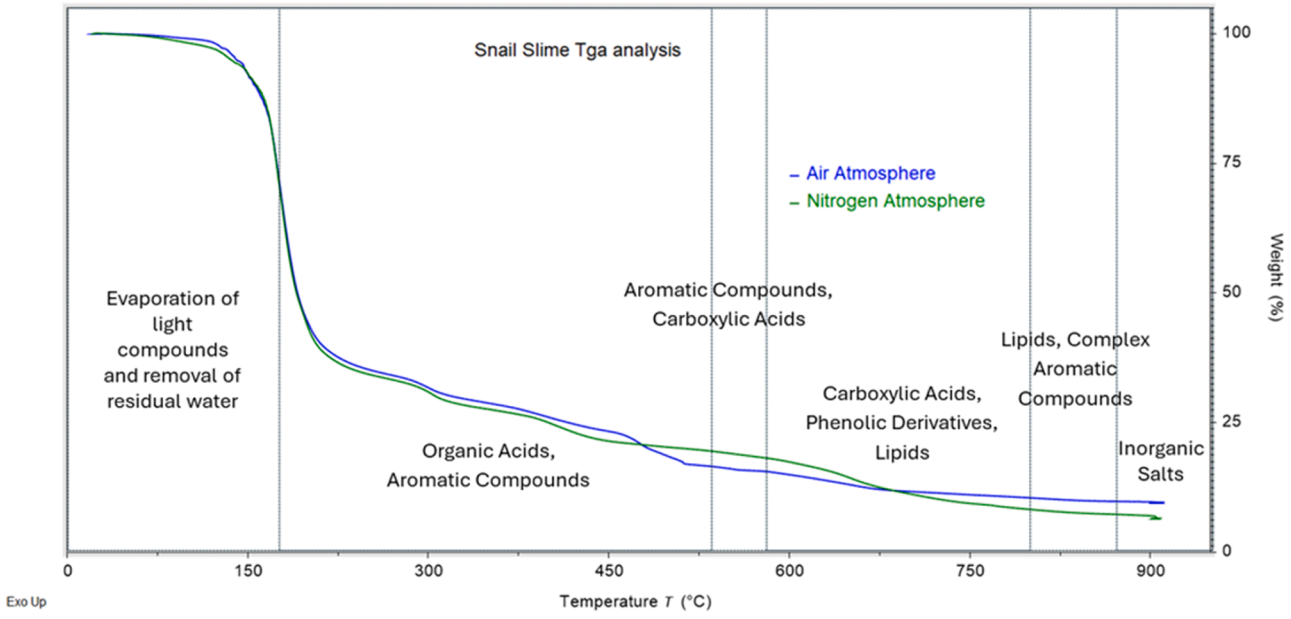

Fig. 5. TGA of freeze-dried SS in air and nitrogen atmospheres. The graph shows the temperature ranges at which different compound families undergo decomposition.

to the combustion of residual carbon and the potential release of inorganic salts such as calcium carbonate, which may be present due to the shell structure of the SS. In nitrogen, non-volatile residues, and inorganic salts may also be released from the sample structure. Overall, in air, oxidation facilitates the complete decomposition of most organic compounds, resulting in a low residue. In contrast, in the N_2 atmosphere, pyrolysis leads to the formation of a higher residue due to incomplete decomposition and the preservation of non-combustible components. The temperature ranges correspond to the decomposition of volatile compounds, organic acids, aromatic compounds, and lipids, as well as the potential release of inorganic salts, highlighting the complex composition of the SS [36,37].

The DSC analyses could not reveal distinct melting temperatures (Tm) and crystallization temperatures (Tc) in both SS and lyophilized SS. However, the structural stability of the samples was assessed across various thermal conditions [38,39].

For the commercial liquid samples, the analyses conducted up to 50°C showed no significant alterations to the structural integrity of the samples observed throughout the cycles (see Fig. 6a). These findings indicate that the liquid formulations maintain their overall stability within this temperature range. In contrast, the lyophilized samples exhibited broader thermal stability (see Fig. 6b). Notably, they maintained their structural integrity up to 70°C, and a melting peak at approximately 81°C was observable just after cycling at 90°C and 100°C. For the sample cycled at 90°C, the enthalpy values (normalized per weight) for Tm and Tc were comparable (3.8244 J/g and 3.6069 J/g, respectively), suggesting that the observed structural changes were non-destructive, likely reflecting a modification of the sample's internal structure rather than complete degradation. Conversely, when the sample was cycled up to 100°C, a more pronounced deviation was noted between the Tm and Tc enthalpy values, with Tm at 6.1383 J/g and Tc at 4.8116 J/g. This suggests that at higher temperatures significant

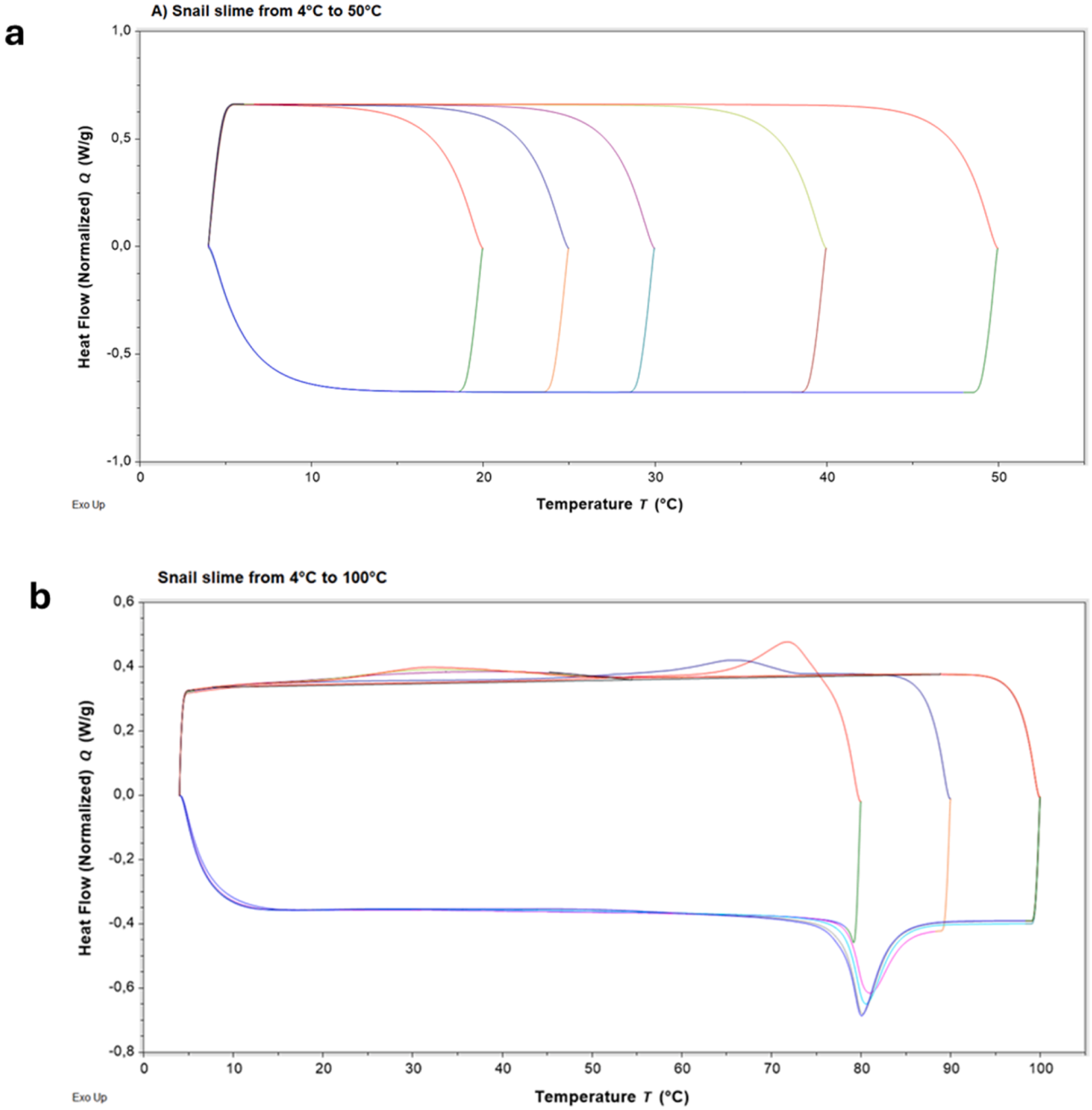

Fig. 6. DSC of stabilized a) liquid and b) lyophilized SS.

changes occurred, due to partial degradation or irreversible structural modifications.

Further cycling of the lyophilized samples to 100°C revealed that, although the Tm values remained relatively stable across cycles, the Tc values varied both in terms of peak shape and enthalpy value. These variations underline the complex thermal behavior of the lyophilized formulations and highlight the impact of repeated thermal cycling on the stability of the samples [40,41].

3.6. Antioxidant results

The discovery of new sources of phenolic compounds has recently attracted the attention of the cosmetics and pharmaceutical industries. In this sense, some researchers have focused on the phenolic compounds in snails' slime. In this study, we determined the total phenolic content of a sample of SS. The total phenolic content of the stabilized slime (2.56 mg GAE/g) was higher than that of the non-stabilized slime (1.48 mg GAE/g) and this may be due to the preservative effects of the stabilizers over time (Figure 7). In a previous study by Alkhadhrh et al. [42], the total phenolic content of *H. aspersa* slime was found to be 150.28 mg of GAE/g extract. In another study by Aouji et al. [12] total phenolic levels of *H. aspersa* snails ranged from 0.16 mg/g of dry matter (in the chloroform extract) to 1.26 mg /g of dry matter (in the ethanol extract).

Antioxidant compounds are key players in protecting against attacks by free radicals, particularly reactive oxygen species. In this sense, antioxidants are considered as an efficient ingredient for enhancing food shelf-life and promoting health [43]. Several compounds are used as antioxidants in food and pharmaceutical products, but most have undesirable side effects such as toxicity. In that sense, we need to replace synthetic ones with natural ones. In this study, the antioxidant activity of *H. aspersa* was investigated in various assays including radical inhibition (ABTS and DPPH), reduction (CUPRAC, FRAP and PBD) and chelation with metal. The results are summarized in Fig. 7. In free radical scavenging assays, the stabilized sample was active and scavenged DPPH (3.14 mg TE/g) and ABTS (0.62 mg TE/g). However, the non-stabilized sample did not show any effect on the scavenging of ABTS and DPPH. In a previous study by Kandeil and Mona [10], the radical scavenging effects of garden and desert snail's slime were investigated by DPPH assay and the desert snail's slime was more active than garden snail's slime. In addition, Alkhadhrh et al. [42] reported that the IC_{50} values for DPPH and ABTS scavenging abilities of *H. aspersa* snail were 20.1 μg/mL and 19.57 μg/mL, respectively. Auoji et al. [12] tested the antioxidant abilities of the extracts of *H. aspersa* snails by several assays and found that the ethanol extract had the highest DPPH scavenging ability (89.36 %). Reducing ability is an important marker for assessing antioxidant properties of natural or synthetic samples. For this purpose, CUPRAC, FRAP and phosphomolybdenum assays were carried out. In all reducing power assays, the stabilized sample exhibited higher ability than the non-stabilized sample. A significant reduction of iron in ethanol extract from *H. aspersa* snail (IC_{50}: 67.98 μg/mL) has been also reported by Auoji et al. [12]. Unlike other antioxidant assays, the ability of non-stabilized snails to chelate metals (5.41 mg EDTAE/g) was greater than that of the stabilized sample (3.23 mg EDTAE/g). The observed metal chelating capacity of the non-stabilized sample can be explained by the high citrate content, which is also known as the active metal chelator [44,45]. As an insight into the structural ability, the superior enhanced radical scavenging and reduction capacity of the stabilized snail may be explained by the presence of benzoic acid and 2,4-dimethylbenzaldehyde [46,47]. In a study Szwajgier et al [47], benzoic acid and 2,4-dimethylbenzaldehyde exhibited moderate DPPH radical scavenging and ferric reducing abilities. The presence of a hydroxyl group in the benzoic acid structure may contribute to its radical scavenging and reducing properties. For example, Velika and Kron [48] evaluated fourteen derivatives of benzoic acid for their efficacy against the superoxide radical, finding that the number and specific position (*para, meta*, or *ortho*) of hydroxyl groups on the benzene ring influenced their ability to scavenge superoxide. Similarly, Chen et al [46] reported the number and position of methoxy and carboxylic acid groups in benzene rings can affect the antioxidant effects of the phenolic constituents. The methyl substituents in 2,4-dimethylbenzaldehyde may also be effective as hydrogen or electron donors.

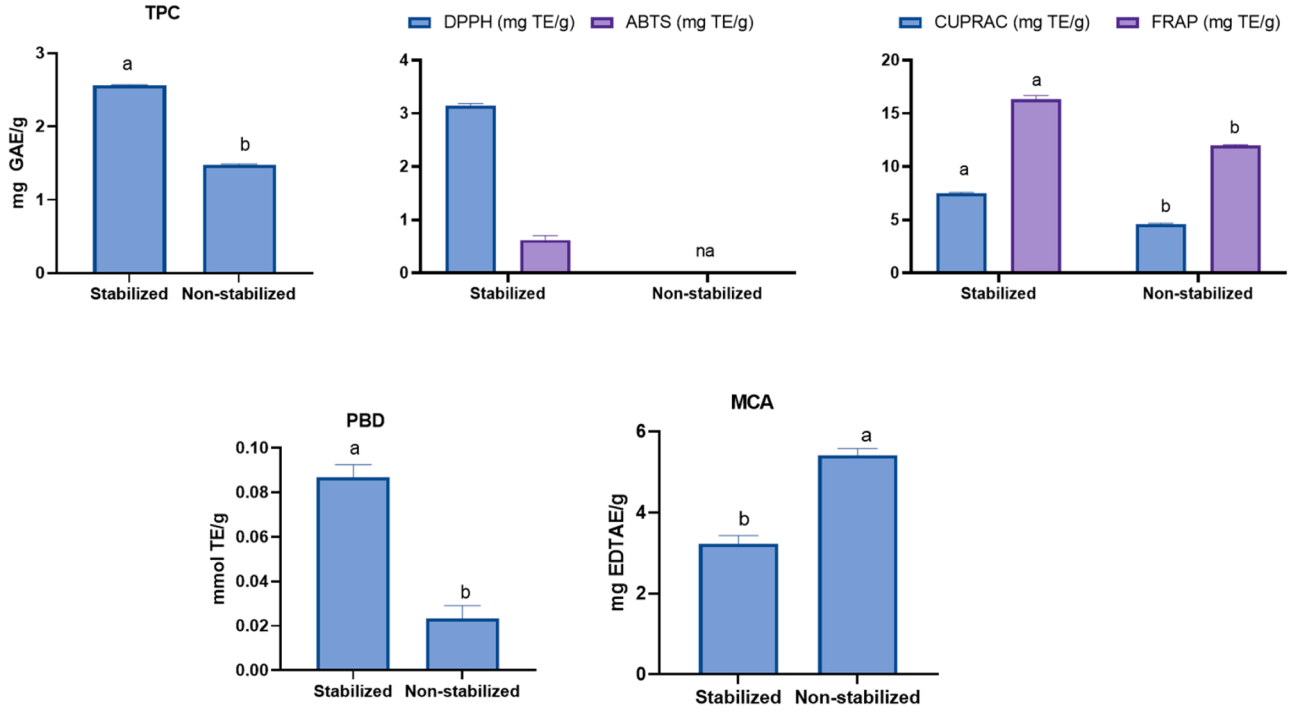

Fig. 7. Total phenolic content (TPC) and antioxidant properties of SS. Values are reported as mean ± SD of three parallel measurements. PBD: Phosphomolybdenum; TE: Trolox Equivalent; EDTAE: EDTA equivalent; na: not active. Different letters indicate significant differences between the samples ($p<0.05$).

3.7. Enzyme inhibition results

The inhibition of key enzymes may be associated with the treatment of global health problems, including obesity, Alzheimer's disease, and diabetes. In this sense, several compounds have been proposed as enzyme inhibitors of the target enzymes [49]. For example, galantamine is known to be one of the most widely used inhibitors of acetylcholine hydrolysis enzyme activity in Alzheimer's patients [50,51]. Acarbose is also used as an inhibitor of amylase and glucosidase and is one of the active ingredients of oral antidiabetic medicinal products [52,53]. Synthetic inhibitors, however, have undesirable side effects in long-term use. Therefore, safe and efficient sources of enzyme inhibitors should be replaced by natural inhibitors. In the current study, we examined enzyme inhibitory properties of snail samples against glucosidase, cholinesterase, amylase and tyrosinase. The results are summarized in Fig. 8. Although the tested snail's slime samples showed similar BChE inhibitory effects, non-stabilized samples were not active on AChE. In addition, the tyrosinase inhibition of stabilized SS sample (21.54 mg KAE/g) was higher than non-stabilized sample (20.85 mg KAE/g). Similarly, amylase inhibition was observed in the SS samples, whereas only non-stabilized sample was active for glucosidase. Limited information regarding the enzyme inhibitory effects of snail's slime has been documented in the literature. In a previous work by Alkhadhrh et al. [42], the tyrosinase inhibitory action of *H. aspersa* snail mucus was reported with an IC_{50} of 35 μg/mL. According to Table 2, the presence of benzoic acid in stabilized slime can be ascribed to its enzyme inhibiting characteristics [54–56]. For example, Liu, et al [57] identified benzoic acid as a strong inhibitor of mushroom tyrosinase, demonstrating a non-competitive mode of action. In another study conducted by Guan et [54], benzoic acid and its derivatives were tested for anti-amylase action and benzoic acid exhibited weak anti-amylase effect with the IC_{50}= 45.25 mM. Additionally, the authors often mentioned that benzene ring with more hydroxyl groups usually improves the ability of the compounds to inhibit amylase. Budryn et al [58] examined the inhibitory effects of hydroxybenzoic acid derivatives on cholinesterase and found that the hydrophobic characteristics of benzene rings may enhance these inhibitory effects. In addition, the presence of benzoic acid, 2, 5-furandione, 3-methyl can interact with enzymes by covalently or non-covalently modifying functional amino groups (typically lysine residues) in proteins and enzymes, and thus enzymatic activity can be inhibited [59]. Thus, the SS samples may serve as an alternate source of natural enzyme inhibitors in place of synthetic inhibitors.

3.8. Biological evaluation

Considering the growing use of SS in dermatological formulations, its impact on dermal fibroblasts was determined by MTT assay measuring the cell metabolic activity and, indirectly, cell viability. NHDFs were treated with three different concentrations of SS, 1:40, 1:60, and 1:80 up to 48 h. After 24 h, cells exposed to SS 1:40 and 1:80 dilutions show a significant increase in cell viability compared to control. After 48 h of treatment, this trend appears even more pronounced and all the SS dilutions (1:40, 1:60, 1:80) lead to record a marked and significant increase in cell metabolic activity with respect to control (Fig. 9).

In our previous study, we tested the SS on human gingival fibroblast

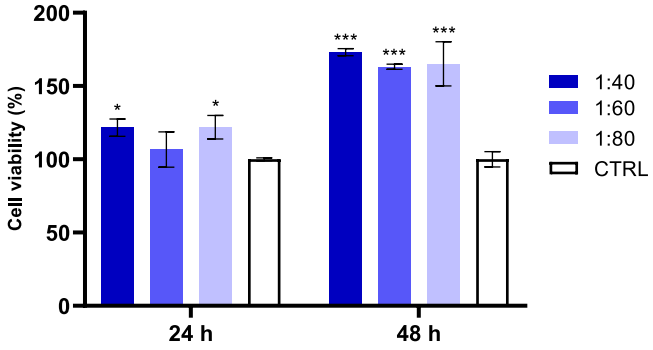

Fig. 9. MTT test performed on NHDFs treated with different dilutions of SS (1:40, 1:60, 1:80) for 24 and 48 h. The reported percentage of viable cells is relative to the control and adjusted at 100 %. Bars show the mean ± SD versus control. For 24 h *vs CTRL $p<0.05$; for 48 h ***vs CTRL $p<0.0001$.

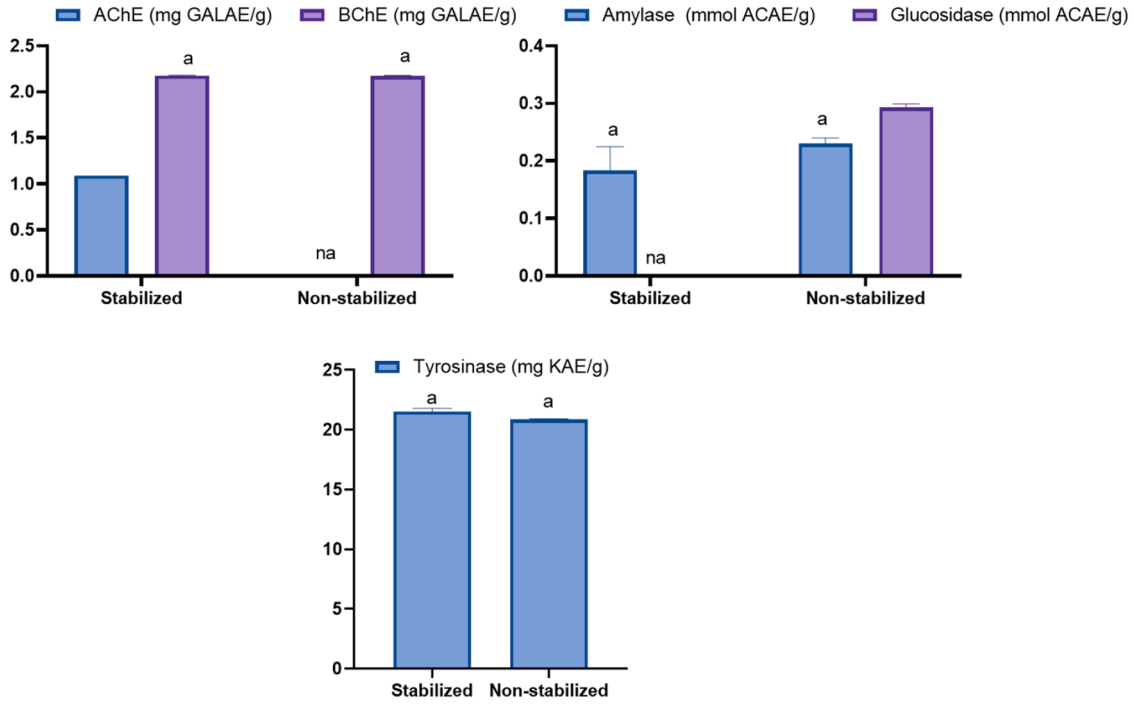

Fig. 8. Enzyme inhibition properties of SS. Values are reported as mean ± SD of three parallel measurements. GALAE: Galantamine equivalent; ACAE: Acarbose equivalent; KAE: Kojic acid equivalent; na: not active. Different letters indicate significant differences between the samples ($p<0.05$).

(HGFs) cells under the same conditions, and a significant increase in cell viability was observed [1]. Given the emerging application of SS in cosmetic formulations, this study evaluated its effect on the viability of the more represented cells of the dermis layer, represented by NHDFs. The results demonstrated a higher cell viability compared to HGFs, with a marked increase after 48 hours, suggesting favorable biocompatibility and cellular acceptance, also confirmed by Deng et al. [60]. Trapella and his colleagues [5] also confirm that SS is non-toxic and well-tolerated by skin and significantly increases the fibroblast viability. Our results are coherent with the previous findings stating that SS is well tolerated by cells populating connective tissues demonstrating an appreciable capability to promote cell viability [1].

4. Conclusion

This study highlights a detailed chemical and biological characterization of *H. aspersa* SS, highlighting its bioactive potential. The results confirm that SS is rich in metabolites with antimicrobial, antioxidant, and enzyme-inhibitory properties. The presence of key compounds such as glycoproteins, organic acids, and phenolic derivatives supports its use in dermatology and pharmaceutical applications. Additionally, the positive impact of preservatives on SS composition and bioactivity suggests that processing methods influence its therapeutic properties. By integrating a multimethod analytical approach with biological assays, this work establishes a direct correlation between chemical composition and functional properties, thereby reinforcing the significance of SS as a versatile natural biomaterial for biomedicine and cosmetics, paving the way for further studies to optimize its applications in health and material sciences.

Funding

This publication was produced during M.R.'s attendance at the PhD program in Biomolecular and Pharmaceutical Sciences at "G. d'Annunzio" University of Chieti-Pescara, Italy, Cycle XXXVIII, with the support of a scholarship financed by the Ministerial Decree no. 351 of 9th April 2022, based on the National Recovery and Resilience Plan (NRRP) - funded by the European Union - NextGenerationEU - Mission 4 "Education and Research", Component 1 "Enhancement of the offer of educational services: from nurseries to universities" - Investment 3.4 "Advanced teaching and university skills".

This publication was produced while S.D.G. was attending the PhD programme in "Biomolecular and Pharmaceutical Sciences" at the University of Chieti-Pescara, Cycle XXXVIII, with the support of a scholarship co-financed by the Ministerial Decree no. 352 of 9th April 2022, based on the NRRP - funded by the European Union – NextGenerationEU - Mission 4 "Education and Research", Component 2 "From Research to Business", Investment 3.3, and by the company Carbotech S.r.l., Via dell'industria, Martinsicuro (TE, Italy).

CRediT authorship contribution statement

Michele Ciulla: Writing – original draft, Software, Resources, Methodology, Formal analysis. **Muhammad Rashad:** Writing – review & editing, Writing – original draft, Methodology, Investigation. **Mattia Spano:** Methodology. **Luisa Mannina:** Investigation. **Stefania Garzoli:** Methodology. **Gokhan Zengin:** Methodology. **Stefano Di Giacomo:** Methodology. **Pantaleone Bruni:** Software, Methodology, Formal analysis. **Pietro Di Profio:** Investigation. **Antonella Fontana:** Validation, Investigation. **Stefania Ferrari:** Visualization, Validation, Data curation. **Amelia Cataldi:** Visualization, Validation. **Simone Carradori:** Writing – review & editing, Writing – original draft, Visualization, Validation, Supervision, Investigation, Funding acquisition, Data curation, Conceptualization. **Susi Zara:** Writing – review & editing, Visualization, Project administration, Funding acquisition, Conceptualization.

Declaration of competing interest

The authors declare no conflict of interest.

Acknowledgments

The results presented in the current paper have been obtained thanks to the collaboration between University "G. d'Annunzio" Chieti-Pescara and Lumacheria Italiana S.r.l. (Cherasco, Italy) in accordance with the agreement signed on 04/02/2025.

Supplementary materials

Supplementary material associated with this article can be found, in the online version, at doi:10.1016/j.molstruc.2025.143838.

Data availability

Data will be made available on request.

References

[1] A. Ricci, M. Gallorini, N. Feghali, S. Sampò, A. Cataldi, S. Zara, Snail Slime Extracted by a Cruelty Free Method Preserves Viability and Controls Inflammation Occurrence: A Focus on Fibroblasts, Molecules 28 (3) (2023) 1222, https://doi.org/10.3390/molecules28031222.
[2] M. Rashad, S. Sampò, A. Cataldi, S. Zara, Biological activities of gastropods secretions: snail and slug slime, Nat. Prod. Bioprospecting 13 (1) (2023) 42, https://doi.org/10.1007/s13659-023-00404-0.
[3] M. Rashad, S. Sampò, A. Cataldi, S. Zara, From Nature to Nurture: The Science and Applications of Snail Slime in Health and Beauty, J. Cosme Dermat. 24 (2) (2025) e70002, https://doi.org/10.1111/jocd.70002.
[4] S. Pitt, M. Graham, C. Dedi, P. Taylor-Harris, A. Gunn, Antimicrobial properties of mucus from the brown garden snail Helix aspersa, Br. J. Biomed. Sci. 72 (4) (2015) 174–181, https://doi.org/10.1080/09674845.2015.11665749.
[5] C. Trapella, R. Rizzo, S. Gallo, A. Alogna, D. Bortolotti, F. Casciano, G. Zauli, P. Secchiero, R. Voltan, HelixComplex snail mucus exhibits pro-survival, proliferative and pro-migration effects on mammalian fibroblasts, Sci. Rep. 8 (1) (2018) 17665, https://doi.org/10.1038/s41598-018-35816-3.
[6] K. Zhu, Z. Zhang, G. Li, J. Sun, T. Gu, N.U. Ain, X. Zhang, D. Li, Extraction, structure, pharmacological activities and applications of polysaccharides and proteins isolated from snail mucus, Int. J. Biol. Macromol. 258 (2024) 128878, https://doi.org/10.1016/j.ijbiomac.2023.128878.
[7] E. Staudacher, Mollusc N-glycosylation: Structures, Functions and Perspectives, Biomolecules 11 (12) (2021), https://doi.org/10.3390/biom11121820.
[8] N. Singh, A.N. Brown, M.H. Gold, Snail extract for skin: A review of uses, projections, and limitations, J. Cosme Dermat. 23 (4) (2024) 1113–1121, https://doi.org/10.1111/jocd.16269.
[9] A. Dolashki, L. Velkova, E. Daskalova, N. Zheleva, Y. Topalova, V. Atanasov, W. Voelter, P. Dolashka, Antimicrobial Activities of Different Fractions from Mucus of the Garden Snail Cornu aspersum, Biomedicines 8 (9) (2020), https://doi.org/10.3390/biomedicines8090315.
[10] M.A. Kandeil, M.M. Mona, Evaluation of antioxidant, antityrosinase, and anticancer activity of mucus extract from both Egyptian land snails, Eremina desertorum and Helix aspersa, with emphasis on their chemical profiles, J. Exp. Zool. A: Ecol. Integr. Physiol. 341 (2) (2024) 182–192, https://doi.org/10.1002/jez.2773.
[11] J. Gubitosa, V. Rizzi, P. Fini, A. Laurenzana, G. Fibbi, C. Veiga-Villauriz, F. Fanelli, F. Fracassi, A. Onzo, G. Bianco, C. Gaeta, A. Guerrieri, P. Cosma, Biomolecules from snail mucus (Helix aspersa) conjugated gold nanoparticles, exhibiting potential wound healing and anti-inflammatory activity, Soft. Matter. 16 (48) (2020) 10876–10888, https://doi.org/10.1039/D0SM01638A.
[12] M. Aouji, A. Rkhaila, B. Bouhaddioui, M. Zirari, H. Harifi, Y. Taboz, L.A. Lrhorfi, R. Bengueddour, Chemical composition, mineral profile, anti-bacterial, and wound healing properties of snail slime of Helix aspersa Müller, Biomed 13 (4) (2023) 10–19, https://doi.org/10.37796/2211-8039.1424.
[13] H.M. Dn, I.L. Kriswandini, Antimicrobial proteins of Snail mucus (Achatina fulica) against Streptococcus mutans and Aggregatibacter actinomycetemcomitans, Dent. J. 47 (1) (2014) 31–36, https://doi.org/10.20473/j.djmkg.v47.i1.p31-36.
[14] J. Zhong, W. Wang, X. Yang, X. Yan, R. Liu, A novel cysteine-rich antimicrobial peptide from the mucus of the snail of Achatina fulica, Peptides 39 (2013) 1–5, https://doi.org/10.1016/j.peptides.2012.09.001.
[15] P. Phrompanya, N. Suriyaruean, N. Nantarat, S. Saenphet, Y. Tragoolpua, K. Saenphet, Biological properties of mucus from land snails (Lissachatina fulica) and freshwater snails (Pomacea canaliculata) and histochemical study of mucous cells in their foot, PeerJ 11 (2023) e15827, https://doi.org/10.7717/peerj.15827.
[16] N.G. Vassilev, S.D. Simova, M. Dangalov, L. Velkova, V. Atanasov, A. Dolashki, P. Dolashka, An (1)H NMR- and MS-Based Study of Metabolites Profiling of Garden

Snail Helix aspersa Mucus, Metabolites 10 (9) (2020), https://doi.org/10.3390/metabo10090360.
[17] A.A.A. Sallam, S.A. El-Massry, I.N. Nasr, Chemical analysis of mucus from certain land snails under Egyptian conditions, Arch. Phytopathol. Plant Prot. 42 (9) (2009) 874–881, https://doi.org/10.1080/03235400701494448.
[18] K. Liudmyla, C. Olena, S. Nadiia, Chemical properties of Helix aspersa mucus as a component of cosmetics and pharmaceutical products, Mater. Today: Proc. 62 (2022) 7650–7653, https://doi.org/10.1016/j.matpr.2022.02.217.
[19] F. Cairone, S. Cesa, I. Arpante, S.C. Di Simone, A.H. Mendez, C. Ferrante, L. Menghini, A. Filippi, C. Fraschetti, G. Zengin, S. Carradori, M. Gallorini, L. Mannina, M. Spano, Pomegranate Juices: Analytical and Bio-Toxicological Comparison of Pasteurization and High-Pressure Processing in the Development of Healthy Products, Foods 14 (2) (2025) 315, https://doi.org/10.3390/foods14020315.
[20] K. Slinkard, V.L. Singleton, Total phenol analysis: automation and comparison with manual methods, Am. J. Enol. Vitic. 28 (1) (1977) 49–55, https://doi.org/10.5344/ajev.1977.28.1.49.
[21] A.J. Kirby, R.J. Schmidt, The antioxidant activity of Chinese herbs for eczema and of placebo herbs—I, J. Ethnopharmacol. 56 (2) (1997) 103–108, https://doi.org/10.1016/S0378-8741(97)01510-9.
[22] T.C. Shekhar, G. Anju, Antioxidant activity by DPPH radical scavenging method of Ageratum conyzoides Linn. leaves, Am. J. ethnomed. 1 (4) (2014) 244–249.
[23] A.L. Dawidowicz, D. Wianowska, M. Olszowy, On practical problems in estimation of antioxidant activity of compounds by DPPH method (Problems in estimation of antioxidant activity), Food Chem. 131 (3) (2012) 1037–1043, https://doi.org/10.1016/j.foodchem.2011.09.067.
[24] R. Re, N. Pellegrini, A. Proteggente, A. Pannala, M. Yang, C. Rice-Evans, Antioxidant activity applying an improved ABTS radical cation decolorization assay, Free Radic. Biol. Med. 26 (9-10) (1999) 1231–1237, https://doi.org/10.1016/S0891-5849(98)00315-3.
[25] R. Apak, K. Güçlü, M. Özyürek, S.E. Karademir, Novel total antioxidant capacity index for dietary polyphenols and vitamins C and E, using their cupric ion reducing capability in the presence of neocuproine: CUPRAC method, J. Agric. Food Chem. 52 (26) (2004) 7970–7981, https://doi.org/10.1021/jf048741x.
[26] I.F. Benzie, J.J. Strain, The ferric reducing ability of plasma (FRAP) as a measure of "antioxidant power": the FRAP assay, Anal. Biochem. 239 (1) (1996) 70–76, https://doi.org/10.1006/abio.1996.0292.
[27] P. Prieto, M. Pineda, M. Aguilar, Spectrophotometric quantitation of antioxidant capacity through the formation of a phosphomolybdenum complex: specific application to the determination of vitamin E, Anal. Biochem. 269 (2) (1999) 337–341, https://doi.org/10.1006/abio.1999.4019.
[28] T.C. Dinis, V.M. Madeira, L.M. Almeida, Action of phenolic derivatives (acetaminophen, salicylate, and 5-aminosalicylate) as inhibitors of membrane lipid peroxidation and as peroxyl radical scavengers, Arch. Biochem. Biophys. 315 (1) (1994) 161–169, https://doi.org/10.1006/abbi.1994.1485.
[29] G.L. Ellman, K.D. Courtney, V. Andres Jr, R.M. Featherstone, A new and rapid colorimetric determination of acetylcholinesterase activity, Biochem. Pharmacol. 7 (2) (1961) 88–95, https://doi.org/10.1016/0006-2952(61)90145-9.
[30] T. Masuda, D. Yamashita, Y. Takeda, S. Yonemori, Screening for tyrosinase inhibitors among extracts of seashore plants and identification of potent inhibitors from Garcinia subelliptica, Biosci. Biotechnol. Biochem. 69 (1) (2005) 197–201, https://doi.org/10.1271/bbb.69.197.
[31] I. Šafašík, Rapid Detection of Alpha-Amylase Inhibitors, J. Enzyme Inhib. 3 (3) (1990) 245–247, https://doi.org/10.3109/14756369009035843.
[32] L. Ting, X.-d. Zhang, Y.-w. Song, J.-w. Liu, A microplate-based screening method for alpha-glucosidase inhibitors, Chin. J. Clin. Pharmacol. Ther. 10 (10) (2005) 1128.
[33] A. Onzo, R. Pascale, M.A. Acquavia, P. Cosma, J. Gubitosa, C. Gaeta, P. Iannece, Y. Tsybin, V. Rizzi, A. Guerrieri, R. Ciriello, G. Bianco, Untargeted analysis of pure snail slime and snail slime-induced Au nanoparticles metabolome with MALDI FT-ICR MS, J. Mass Spectrom. 56 (5) (2021) e4722, https://doi.org/10.1002/jms.4722.
[34] A. Alogna, V. Gentili, C. Trapella, S.S. Hallan, M. Sguizzato, G. Strazzabosco, M. Fernández, R. Cortesi, R. Rizzo, D. Bortolotti, Design of Liposomes Carrying HelixComplex Snail Mucus: Preliminary Studies, Molecules 26 (16) (2021) 4709, https://doi.org/10.3390/molecules26164709.
[35] Y. Wang, L. Jia, J. Guo, B. Wang, L. Zhang, J. Xiang, Y. Jin, Thermogravimetric analysis of co-combustion between municipal sewage sludge and coal slime: Combustion characteristics, interaction and kinetics, Thermochim. Acta 706 (2021) 179056, https://doi.org/10.1016/j.tca.2021.179056.
[36] M.F. Di Filippo, L.S. Dolci, F. Bonvicini, F. Sparla, G.A. Gentilomi, S. Panzavolta, N. Passerini, B. Albertini, Influence of the extraction method on functional properties of commercial snail secretion filtrates, Scie Repor 14 (1) (2024) 22053, https://doi.org/10.1038/s41598-024-72733-0.
[37] R. Dong, Z. Tang, H. Song, Y. Chen, X. Wang, H. Yang, H. Chen, Co-pyrolysis of vineyards biomass waste and plastic waste: Thermal behavior, pyrolytic characteristic, kinetics, and thermodynamics analysis, J. Anal. Appl. Pyrolysis. 179 (2024) 106506, https://doi.org/10.1016/j.jaap.2024.106506.
[38] M. Sheng, D. Valco, C. Tucker, E. Cayo, T. Lopez, Practical Use of Differential Scanning Calorimetry for Thermal Stability Hazard Evaluation, Org. Process. Res. Dev. 23 (10) (2019) 2200–2209, https://doi.org/10.1021/acs.oprd.9b00266.
[39] F.-L. Obas, L.C. Thomas, M.W. Terban, S.J. Schmidt, Characterization of the thermal behavior and structural properties of a commercial high-solids confectionary gel made with gelatin, Food Hydrocoll. 148 (2024) 109432, https://doi.org/10.1016/j.foodhyd.2023.109432.
[40] J. Wen, K. Arthur, L. Chemmalil, S. Muzammil, J. Gabrielson, Y. Jiang, Applications of Differential Scanning Calorimetry for Thermal Stability Analysis of Proteins: Qualification of DSC, J. Pharm. Sci. 101 (3) (2012) 955–964, https://doi.org/10.1002/jps.22820.
[41] I. Maule, G. Razzetti, A. Restelli, A. Palmieri, C. Colombo, R. Ballini, Thermal Stability Evaluation of Nitroalkanes with Differential Scanning Calorimetry, Org. Process. Res. Dev. 25 (4) (2021) 781–788, https://doi.org/10.1021/acs.oprd.0c00433.
[42] M. Alkhadhrh, R. Issa, L.K. Al-Halaseh, L. Alnsour, A. Alsarayreh, Y. Al Qaisi, S. M. Matalqah, S. Aladwan, Investigating the inhibitory effects of carotenoids-fortified Helix aspersa slime on oxidative stress, collagenase and tyrosinase enzyme activities, J. Cosmet. Dermatol. 23 (11) (2024) 3757–3766, https://doi.org/10.1111/jocd.16455.
[43] B. Halliwell, Understanding mechanisms of antioxidant action in health and disease, Nat. Rev. Mol. Cell Biol. 25 (1) (2024) 13–33, https://doi.org/10.1038/s41580-023-00645-4.
[44] Y.C. Shinta, B. Zaman, S. Sumiyati, Citric Acid and EDTA as chelating agents in phytoremediation of heavy metal in polluted soil: a review, IOP Conf. Ser.: Earth Environ. Sci. 896 (1) (2021) 012023, https://doi.org/10.1088/1755-1315/896/1/012023.
[45] G. Mattar, A. Haddarah, J. Haddad, M. Pujola, F. Sepulcre, Are Citric Acid-Iron II Complexes True Chelates or Just Physical Mixtures and How to Prove This? Foods 12 (2) (2023) 410, https://doi.org/10.3390/foods12020410.
[46] J. Chen, J. Yang, L. Ma, J. Li, N. Shahzad, C.K. Kim, Structure-antioxidant activity relationship of methoxy, phenolic hydroxyl, and carboxylic acid groups of phenolic acids, Sci. Rep. 10 (1) (2020) 2611, https://doi.org/10.1038/s41598-020-59451-z.
[47] D. Szwajgier, J. Pielecki, Z. Targoński, Antioxidant activities of cinnamic and benzoic acid derivaties, Acta Sci. Pol. Technol. Aliment. 4 (2) (2005) 129–142.
[48] B. Velika, I. Kron, Antioxidant properties of benzoic acid derivatives against Superoxide radical, Free Radic. Antioxid. 2 (4) (2012) 62–67, https://doi.org/10.5530/ax.2012.4.11.
[49] A. Rauf, N. Jehan, Natural Products as a Potential Enzyme Inhibitors from Medicinal Plants, in: M. Şentürk (Ed.), Enzyme Inhibitors and Activators, IntechOpen, Rijeka, 2017, 10.5772/67376.
[50] H. Nour, O. Abchir, N. Mounadi, A. Samadi, B. Salah, S. Chtita, Exploration of natural products for the development of promising cholinesterase inhibitors in Alzheimer's disease treatment, Heliyon 11 (4) (2025) e42479, https://doi.org/10.1016/j.heliyon.2025.e42479.
[51] M. Saadullah, A. Farid, A. Ali, M. Rashad, F. Naseem, S.A. Rashid, S. Ghazanfar, M. Yasin, N. Akhtar, M.S. Almuhayawi, Molecular modeling study of novel lancifolamide bioactive molecule as an inhibitor of acetylcholinesterase (AChE), herpes simplex virus (HSV-1), and anti-proliferative proteins, Molecules 27 (17) (2022) 5480, https://doi.org/10.3390/molecules27175480.
[52] A. Kumar, V.Kumar Singh, A.M. Kayastha, Studies on α-amylase inhibition by acarbose and quercetin using fluorescence, circular dichroism, docking, and dynamics simulations, Spectrochim. Acta A: Mol. Biomol. Spectrosc. 314 (2024) 124160, https://doi.org/10.1016/j.saa.2024.124160.
[53] M. Saadullah, M. Asif, M. Uzair, S. Afzal, S.A. Rashid, M. Rashad, R. Bashir, S. Mahmood, Pharmacological evaluation of the hypoglycemic and anti-Alzheimer's activities of aerial parts of Breynia distachia (Phyllanthaceae), Trop. J. Pharm. Res. 21 (3) (2022) 579–587, https://doi.org/10.4314/tjpr.v21i3.18.
[54] L. Guan, H. Long, F. Ren, Y. Li, H. Zhang, A Structure-Activity Relationship Study of the Inhibition of α-Amylase by Benzoic Acid and Its Derivatives, Nutrients 14 (9) (2022), https://doi.org/10.3390/nu14091931.
[55] M. Yildiz, D. Kiliç, Y. Ünver, M. Şentürk, H. Askin, Ö.İ. Küfrevioğlu, Acetylcholinesterase inhibitory properties of some benzoic acid derivatives, in: AIP Conference Proceedings, AIP Publishing LLC, 2016 020102, https://doi.org/10.1063/1.4945928.
[56] Q.-X. Chen, K.-K. Song, L. Qiu, X.-D. Liu, H. Huang, H.-Y. Guo, Inhibitory effects on mushroom tyrosinase by p-alkoxybenzoic acids, Food Chem. 91 (2) (2005) 269–274, https://doi.org/10.1016/j.foodchem.2004.01.078.
[57] L. Xiaodan, H. Huang, C. Qingxi, Studies on inhibitory effects of benzoic acid on mushroom tyrosinase, Xiamen da xue xue bao. Zi ran ke xue ban=, J. Xiamen Univ. Nat. Sci. 42 (1) (2003) 102–106.
[58] G. Budryn, I. Majak, J. Grzelczyk, D. Szwajgier, A. Rodríguez-Martínez, H. Pérez-Sánchez, Hydroxybenzoic acids as acetylcholinesterase inhibitors: Calorimetric and docking simulation studies, Nutrients 14 (12) (2022) 2476, https://doi.org/10.3390/nu14122476.
[59] P.J. Butler, J.I. Harris, B.S. Hartley, R. Lebeman, The use of maleic anhydride for the reversible blocking of amino groups in polypeptide chains, Biochem. J. 112 (5) (1969) 679–689, https://doi.org/10.1042/bj1120679.
[60] T. Deng, D. Gao, X. Song, et al., A natural biological adhesive from snail mucus for wound repair, Nat. Commun. 14 (2023) 396, https://doi.org/10.1038/s41467-023-35907-4.